






Robust Weak Topological Insulator in the Bismuth Halide $\text{Bi}_4\text{Br}_2\text{I}_2$

Ryo Noguchi,^{1,*} Masaru Kobayashi,² Kaishu Kawaguchi,¹ Wataru Yamamori,² Kohei Aido,¹ Chun Lin ¹, Hiroaki Tanaka ¹, Kenta Kuroda ^{1,3,4}, Ayumi Harasawa,¹ Viktor Kandyba,⁵ Mattia Cattelan ⁵, Alexei Barinov,⁵ Makoto Hashimoto,⁶ Donghui Lu,⁶ Masayuki Ochi,^{7,8} Takao Sasagawa,^{2,9,†} and Takeshi Kondo ^{1,10,‡}

¹*Institute for Solid State Physics (ISSP), University of Tokyo, Kashiwa, Chiba 277-8581, Japan*

²*Laboratory for Materials and Structures, Tokyo Institute of Technology, Yokohama, Kanagawa 226-8501, Japan*

³*International Institute for Sustainability with Knotted Chiral Meta Matter (WPI-SKCM²), Hiroshima University, Higashi-hiroshima, Hiroshima 739-8526, Japan*

⁴*Graduate School of Advanced Science and Engineering, Hiroshima University, Higashi-hiroshima, Hiroshima 739-8526, Japan*

⁵*Eletra—Sincrotrone Trieste, S.S.14, 163.5 km, Basovizza, Trieste, Italy*

⁶*Stanford Synchrotron Radiation Light source, SLAC National Accelerator Laboratory, 2575 Sand Hill Road, Menlo Park, California 94025, USA*

⁷*Department of Physics, Osaka University, 1-1 Machikaneyama-cho, Toyonaka, Osaka 560-0043, Japan*

⁸*Forefront Research Center, Osaka University, 1-1 Machikaneyama-cho, Toyonaka, Osaka 560-0043, Japan*

⁹*Research Center for Autonomous Systems Materialogy, Tokyo Institute of Technology, Yokohama, Kanagawa 226-8501, Japan*

¹⁰*Trans-scale Quantum Science Institute, The University of Tokyo, Tokyo 113-0033, Japan*



(Received 17 January 2023; accepted 9 July 2024; published 22 August 2024)

We apply a topological material design concept for selecting a bulk topology of 3D crystals by different van der Waals stackings of 2D topological insulator layers, and find a bismuth halide $\text{Bi}_4\text{Br}_2\text{I}_2$ to be an ideal weak topological insulator (WTI) with the largest band gap (~ 300 meV) among all the WTI candidates, by means of angle-resolved photoemission spectroscopy (ARPES), density functional theory (DFT) calculations, and resistivity measurements. Furthermore, we reveal that the topological surface state of a WTI is not “weak” but rather robust against external perturbations against the initial theoretical prediction by performing potassium deposition experiments. Our results vastly expand future opportunities for fundamental research and device applications with a robust WTI.

DOI: [10.1103/PhysRevLett.133.086602](https://doi.org/10.1103/PhysRevLett.133.086602)

Highly directional spin currents flow along side surfaces of crystals in a weak topological insulator [1,2]. The topological spin currents would be more robust against impurity scattering than those in a strong topological insulator (STI) that prohibits only perfect backscattering [3,4]. This is supported by experiments showing that the carrier lifetime of a one-dimensional topological edge state could be even two orders longer than that of STIs [4]. WTIs, thus, could be even more advantageous than STIs for various applications. In contrast to STIs, however, the materials hosting WTI states are very scarce [5–14]. In addition, the WTIs established so far have a band gap relatively smaller than those of STIs reaching up to ~ 300 – 350 meV [15]. It may make the WTI states fragile against excitations and difficult to extract without being masked by the nontrivial bulk contributions. Therefore, the

discovery of a WTI with a large band gap has been awaited in materials science.

A difficulty in searching for WTIs comes from their property that the topological surface state (TSS) resides only on the side surface of crystals that are usually not cleavable, preventing the verification of their bulk band topology. Another difficulty is finding an insulator, not a semimetal, hosting a WTI state. This is a required condition to utilize TSSs for research and application without contamination of trivial bulk conductivity. So far, only four compounds have been proposed as WTIs via experiments: $\text{Bi}_{14}\text{Rh}_3\text{I}_9$, $\beta\text{-Bi}_4\text{I}_4$, ZrTe_5 , and HfTe_5 [6,10–12]. $\text{Bi}_{14}\text{Rh}_3\text{I}_9$ has a relatively large band gap (~ 200 meV), whereas the other three have small ones (~ 100 , ~ 30 , and ~ 50 meV each). $\text{Bi}_{14}\text{Rh}_3\text{I}_9$ is a promising candidate for a WTI with a large gap. However, the side surface of this compound is not cleavable, preventing the direct observation of the topological surface band required for the identification of a WTI.

Recently, quasi-one-dimensional (quasi-1D) bismuth halides Bi_4X_4 ($X = \text{Br}, \text{I}$) have attracted much attention as a versatile platform to realize various topological phases [9,12,13,16–36]. These compounds can be regarded as the

*Present address: Department of Physics and Institute for Quantum Information and Matter, California Institute of Technology, Pasadena, California 91125, USA.

†Contact author: sasagawa.t.aa@m.titech.ac.jp

‡Contact author: kondo1215@issp.u-tokyo.ac.jp

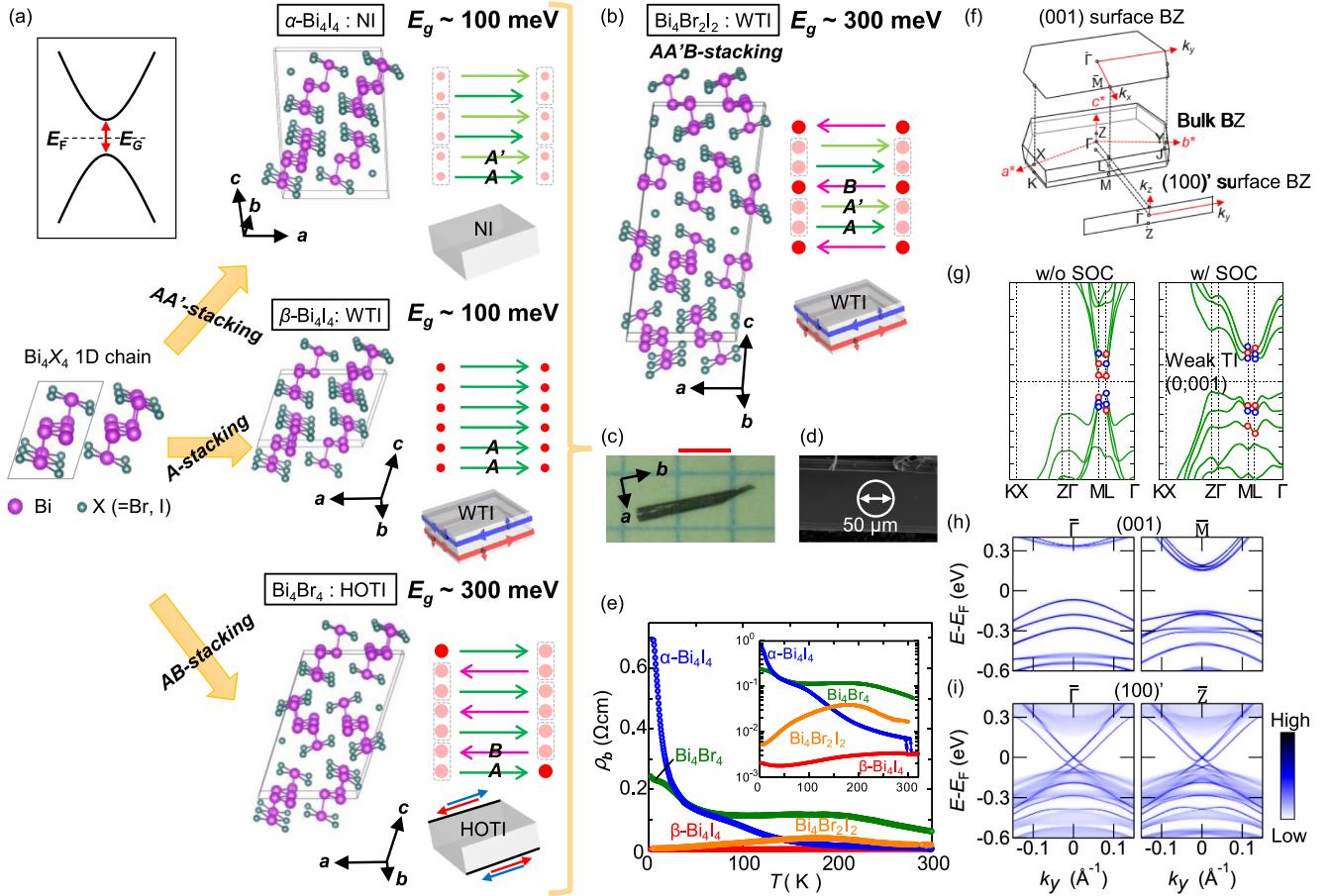


FIG. 1. Topological material design concept. (a) Topological phases selected by different van der Waals stackings of Bi₄X₄ (X = Br, I) chains. A NI, a WTI, and a HOTI have been experimentally validated in A stacking (α-Bi₄I₄), AA' stacking (β-Bi₄I₄), and AB stacking (Bi₄Br₄), respectively. (b) The trilayer Bi₄Br₂I₂ built from AA'B stacking. Topological spin currents and the annihilated ones are expressed by densely and lightly painted circles. (c) Photograph of a Bi₄Br₂I₂ crystal. The scale bar is 1 mm. (d) Scanning electron microscope (SEM) image of a cleaved surface. (e) The resistivity of Bi₄Br₂I₂, compared with other related compounds. (f) Brillouin zone (BZ) for the bulk and projected surfaces of AA'B-stacked Bi₄X₄. (g) Bulk band calculations of Bi₄Br₂I₂ with and without SOC. The red and blue circles indicate even and odd parities, respectively. (h),(i) Calculated surface spectral weights for the top plane (001) and the side plane (100)', respectively.

stacking of two-dimensional TIs (2D TIs) [16], and several types of stacking structures realizing different bulk topologies have been proposed. The crystals built from chains can be easily cleaved by Scotch tape along both top and side surfaces, allowing one to observe topological boundary states.

So far, three types of crystal structures (α-Bi₄I₄, β-Bi₄I₄, and Bi₄Br₄) have been investigated by theory and experiments [Fig. 1(a)], and each has been experimentally identified as a normal insulator (NI), a WTI, and a higher-order topological insulator (HOTI). The band gap of the WTI (β-Bi₄I₄) is, however, rather small (~100 meV [12]), compared to that of Bi₄Rh₃I₉ (~200 meV). In this Letter, we find the trilayer Bi₄Br₂I₂ to be a weak topological insulator with the largest band gap of ~300 meV among all WTIs. We furthermore demonstrate that the topological surface state of a WTI is robust against external

perturbation by the potassium deposition experiments, similarly to the case of a STI.

Theoretically, the monolayer Bi₄Br₄ has a larger band gap than the monolayer Bi₄I₄ [16]. The band gap of the layer-stacked 3D crystal could also be enlarged by substituting I for Br in Bi₄I₄. The Bi₄Br₄ crystal, indeed, shows a large band gap (~300 meV) [27]. It is, however, double layered with the AB stacking, which hosts a HOTI, not a WTI. Bi₄Br₄ built from a single-layered A stacking has been theoretically suggested as a WTI [9]. Nevertheless, such crystals are not stable and cannot be synthesized. One needs an alternative structure realizing a WTI that can be synthesized and still take advantage of Bi₄Br₄ layers with a large band gap.

We find Bi₄Br₂I₂ with AA'B stacking to fulfill such a condition [Figs. 1(b)–1(d)] [37,38]. This structure can be viewed as an alternative stacking of AA' layers and a B

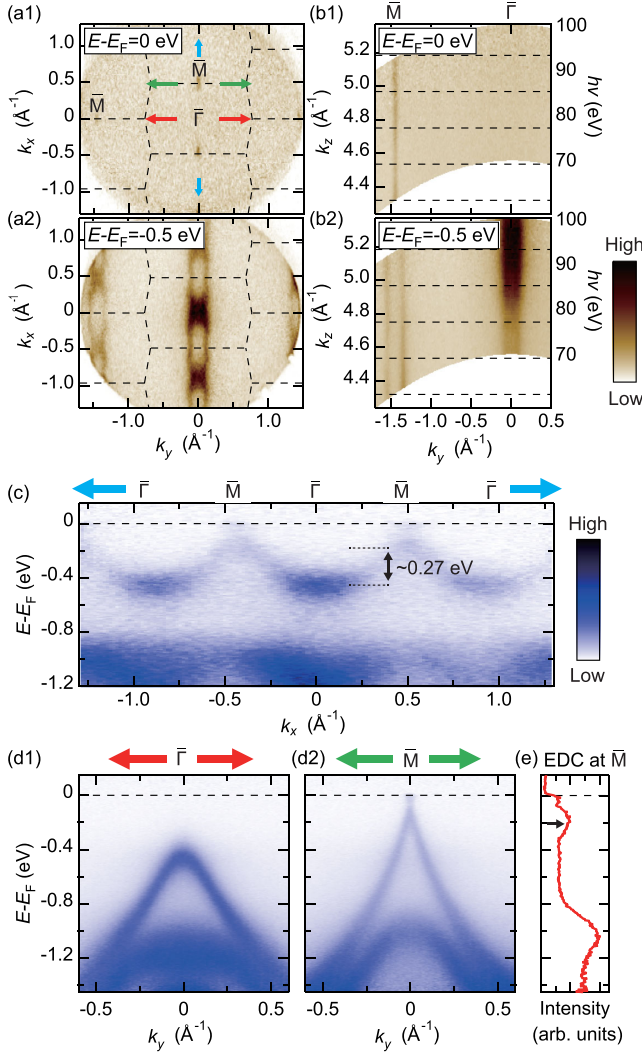


FIG. 2. Synchrotron-ARPES data showing the bulk band. (a1), (a2) ARPES maps along k_y - k_x at $E - E_F = 0$ and -0.5 eV, respectively ($h\nu = 100$ eV). (b1),(b2) ARPES maps along k_y - k_z at $E - E_F = 0$ and -0.5 eV, respectively. Bulk band dispersions along the \bar{M} - $\bar{\Gamma}$ - \bar{M} cut (c) and across $\bar{\Gamma}$ and \bar{M} (d1),(d2) ($h\nu = 100$ eV). (e) Energy distribution curve (EDC) at \bar{M} extracted from (d2). The black arrow indicates the valence band top. The sample temperature was 20 K.

layer mutually flipped by 180 degrees. Since the AA' layers should behave as normal insulators, as in α - Bi_4I_4 , the $AA'B$ -stacked structure can be viewed as 2D TI layers (B layers) alternatively stacked with insulator blocks (AA' layers). In the band structure [Fig. 1(g)], only a single parity inversion becomes effective when all the trilayer-split bands are inverted by strong spin-orbit interaction. Surface calculations [Figs. 1(h) and 1(i)] indeed predict a topological Dirac dispersion to emerge only on the side surface.

The resistivities [Fig. 1(e)] along chains provide two implications. (1) The resistivity of $\text{Bi}_4\text{Br}_2\text{I}_2$ shows an insulating behavior around room temperature. The

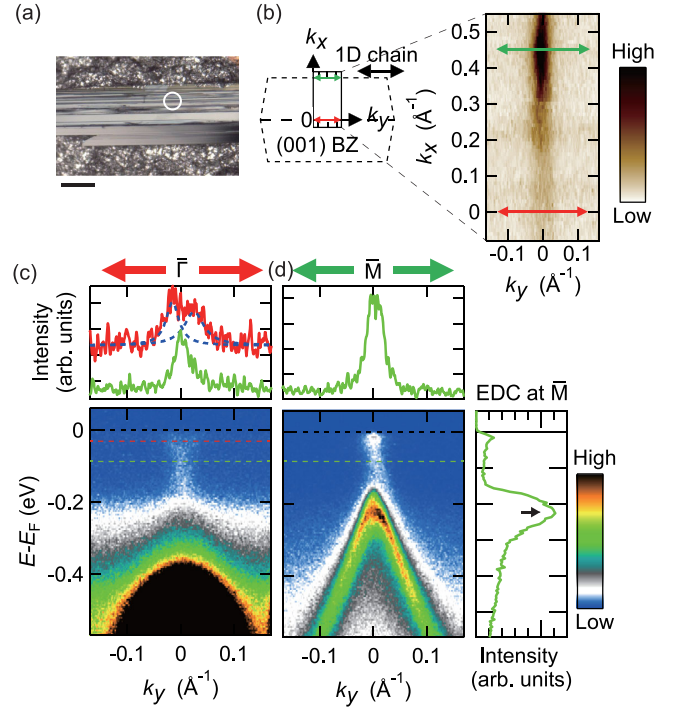


FIG. 3. Laser-ARPES data showing the bulk and surface bands. (a) Photograph of a cleavage surface. The scale bar is 100 μm . The white circle denotes the position observed by ARPES. (b) ARPES map along k_y - k_x at E_F . (c) Band map across $\bar{\Gamma}$ (bottom) and momentum distribution curves (MDCs) (top) for two different binding energies (dashed line in the map). Blue dotted lines are doubled Lorentzian curves. (d) Band map across \bar{M} (bottom), MDC (top), and EDC at \bar{M} (right). The arrow indicates the valence band top. The sample temperature was 30 K.

magnitude comes to between those of Bi_4Br_4 and Bi_4I_4 , indicating that the bulk gap of $\text{Bi}_4\text{Br}_2\text{I}_2$ is smaller than that of Bi_4Br_4 (a HOTI) but larger than α - and β - Bi_4I_4 (a normal insulator and a WTI, respectively). (2) The resistivity of $\text{Bi}_4\text{Br}_2\text{I}_2$ decreases upon cooling below ~ 150 K and turns metallic at low temperatures. The metallic resistivity is much smaller than the low-temperature resistivity of Bi_4Br_4 (a HOTI) and comparable to (smaller, but only slightly than) that of β - Bi_4I_4 . These results imply that $\text{Bi}_4\text{Br}_2\text{I}_2$ is in a topological phase with a large insulating band gap in bulk and massive currents on the surface. Nevertheless, direct observation of the bulk band structure and the topological surface state by ARPES is required to decisively reach this conclusion.

The synchrotron-based ARPES measurements were performed on the ab planes. Typically, the surface is composed of relatively large terraces, larger than the light spot (~ 50 μm), together with a bunch of small steps. ARPES intensity maps along the ab plane at the Fermi level (E_F) [Fig. 2(a1)] show islandlike weak intensities at \bar{M} . Anisotropic features with parallel segments are clarified at higher binding energies [Fig. 2(a2)]. The quasi-1D feature is further confirmed [Figs. 2(b1) and 2(b2)] in

the map of the k_z direction (or the AA' -stacking direction) obtained by changing photon energy.

The bulk valence band is found to disperse in energy by ~ 270 meV along $\bar{M}-\bar{\Gamma}-\bar{M}$ [Fig. 2(c)]. This is similar to that of Bi_4I_4 (~ 260 meV) and smaller than that of Bi_4Br_4 (~ 350 meV) [12,27]. The energy distribution curve (EDC) at \bar{M} [Fig. 2(e)] indicates that the top of the bulk valence band is deep below E_F (marked by an arrow), whereas the bulk conduction band is located above E_F , exhibiting a spectral tail.

We also used laser-based ARPES with high energy and momentum resolutions. To detect the signals of the side surface where TSSs are expected to exist, we illuminate a laser with a $50\ \mu\text{m}$ spot onto a surface portion with many steps [a circle in Fig. 3(a)] with both the (001) top and (100)' side planes. Importantly, we observe a quasi-1D structure [Fig. 3(b)] which forms a Dirac-like dispersion [Figs. 3(c) and 3(d)] inside the bulk band gap that is spin polarized (Supplemental Fig. S3 [38]). It should, therefore, be attributed to a TSS. The gap magnitude at \bar{M} , where the bulk band gap becomes minimal, is estimated to be ~ 230 meV [right panel of Fig. 3(d)]. We should note, however, that this gap value is only the lower limit since the valence band is situated above E_F .

We employed nano-ARPES with a focused photon beam less than $1\ \mu\text{m}$ in spot size for cleaved crystals along the bc and ab surfaces to independently observe the (001) and (100)' planes. Figure 4(b) shows the real-space intensity map of the Bi $5d$ core level for the side bc plane. The Fermi surface map [Fig. 4(c)] shows a quasi-1D feature along k_z

over many Brillouin zones. The energy dispersions [Fig. 4(d)] exhibit metallic in-gap states with almost no variation between the zone center and corner [red and green lines in Fig. 4(c), respectively]. In contrast, the ARPES dispersions [Fig. 4(i)] for the top ab -plane capture the bulk valence band with a clear difference between the zone center and corner [red and green lines in Fig. 4(h)]. These are consistent with the theoretical prediction [Figs. 4(e) and 4(j)].

The larger band gap makes the topological property robust against thermal fluctuations. Nevertheless, the robustness of the WTI phase itself is still controversial. Initially, the topological surface state of a WTI was predicted to be destroyed by disorders, so a WTI was thought of as being literally “weak” in contrast to a strong TI [1,2]. Later, however, theoretical studies pointed out that the surface states of a WTI may not be so fragile due to the protection by time-reversal symmetry [56–58]. However, it has not been tested by experiments to the best of our knowledge. We thus performed the potassium deposition experiments, which apply a strong perturbation by putting impurities and adding a potential gradient on the crystal surface.

For that, we prepared new crystals (see Supplemental Material [38]) with an optimized ratio between Br and I to make it closer to 1 : 1 in the grown crystals. Importantly, we succeeded in increasing the bulk band gap up to ~ 300 meV [Fig. 5(a)], which is the largest among all WTI materials. We also confirmed the topological Dirac dispersion for the side surface of a crystal [Fig. 5(b)].

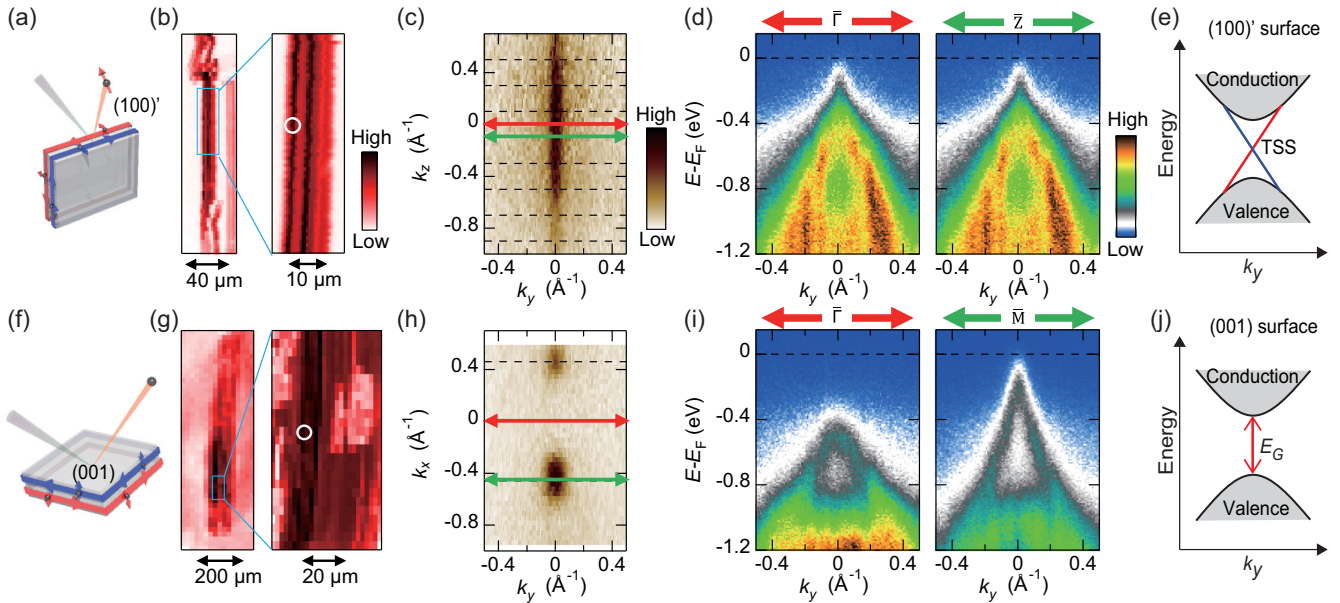


FIG. 4. Selective observation of the top and side surfaces by nano-ARPES. (a) Experimental geometry. (b) Photoemission intensity map in real space. The position measured is indicated by a white circle. (c) ARPES intensity map at E_F . (d) ARPES band maps across two momentum cuts in (c). (e) Schematic of the bulk and surface bands with a TSS. (f)–(j) The same data as (a)–(e), but for the (001) top surface. The sample temperature was 100 K.

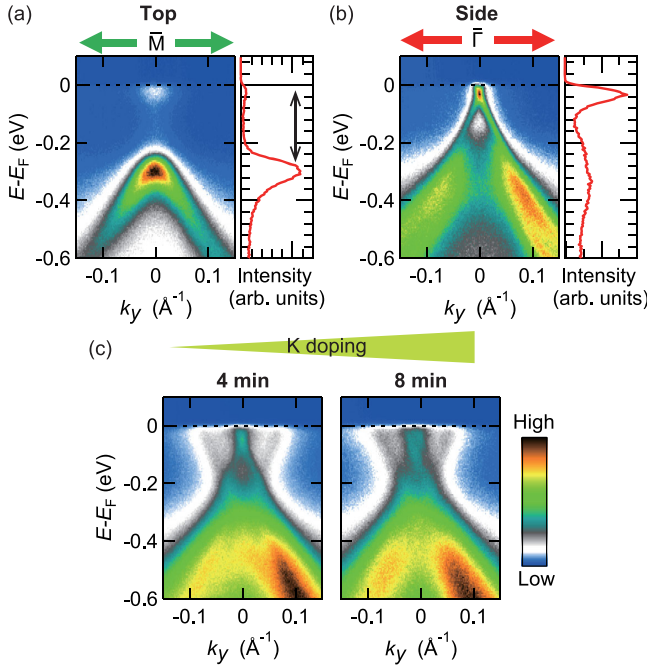


FIG. 5. Potassium deposition experiments for composition optimized crystals. (a),(b) APRES band map around \bar{M} of the (001) top surface and $\bar{\Gamma}$ of the (100)' side surface, respectively. The right panel of each map extracts the EDC at \bar{M} or $\bar{\Gamma}$. (c) The band maps, same as that of (b), but taken after potassium deposition for 4 min (left) and 8 min (right). The sample temperature was 50 K throughout the experiment.

Next, we deposited potassium on the same surface [Fig. 5(c)]. Similarly to the case of Bi_2Se_3 [59,60], the Dirac point is shifted to higher binding energies due to the electron doping and an electronlike band appears below E_F likely due to a quantum well state. Most importantly, the topological Dirac dispersion survives under severe external perturbations (impurity scattering and potential gradient) on the surface, verifying the WTI state is robust, similar to a STI state.

In conclusion, we investigated a trilayer bismuth halide $\text{Bi}_4\text{Br}_2\text{I}_2$, based on the topological material design. $\text{Bi}_4\text{Br}_2\text{I}_2$ was identified as the most robust WTI with the largest band gap (~ 300 meV) among the existing WTIs. The gap size is even comparable to that of Bi_2Se_3 , which is the largest among strong TIs. Very importantly, $\text{Bi}_4\text{Br}_2\text{I}_2$ with the top and side planes both naturally cleavable has advantages overcoming $\text{Bi}_{14}\text{Rh}_3\text{I}_9$ with the second largest bulk gap (~ 200 meV) mainly in two ways. One is that the topological state was identified via direct observation of the topological surface band. Second is that the exfoliation technique can be employed to prepare 1D flakes with spin currents. Furthermore, potassium deposition experiments ensure the robustness of the WTI phase. $\text{Bi}_4\text{Br}_2\text{I}_2$, therefore, has a huge potential, even exceeding that of STIs, for future research and device applications.

Acknowledgments—This work was supported by the JSPS KAKENHI (Grants No. JP18J21892, No. JP21H04652, No. JP21K18181, No. JP21H04439, No. JP23K17351, No. JP21H05236, and No. JP22H01943), by MEXT Q-LEAP (Grant No. JPMXS0118068681), by The Asahi Glass Foundation, by The Murata Science Foundation, and by The Mitsubishi Foundation. Use of the Stanford Synchrotron Radiation Lightsource at the SLAC National Accelerator Laboratory is supported by the U.S. Department of Energy, Office of Science, Office of Basic Energy Sciences under Contract No. DE-AC02-76SF00515. The nano-ARPES experiments were performed with the approval of Elettra Sincrotrone Trieste (Proposal No. 20210361). R. N. acknowledges support by JSPS through the Program for Leading Graduate Schools (ALPS).

- [1] L. Fu and C. L. Kane, Topological insulators with inversion symmetry, *Phys. Rev. B* **76**, 045302 (2007).
- [2] L. Fu, C. L. Kane, and E. J. Mele, Topological insulators in three dimensions, *Phys. Rev. Lett.* **98**, 106803 (2007).
- [3] S. Kim, S. Yoshizawa, Y. Ishida, K. Eto, K. Segawa, Y. Ando, S. Shin, and F. Komori, Robust protection from backscattering in the topological insulator $\text{Bi}_{1.5}\text{Sb}_{0.5}\text{Te}_{1.7}\text{Se}_{1.3}$, *Phys. Rev. Lett.* **112**, 136802 (2014).
- [4] J. Han *et al.*, Optical bulk-boundary dichotomy in a quantum spin Hall insulator, *Sci. Bull.* **68**, 417 (2023).
- [5] B. Yan, L. MÜchler, and C. Felser, Prediction of weak topological insulators in layered semiconductors, *Phys. Rev. Lett.* **109**, 116406 (2012).
- [6] B. Rasche, A. Isaeva, M. Ruck, S. Borisenko, V. Zabolotnyy, B. Büchner, K. Koepernik, C. Ortix, M. Richter, and J. van den Brink, Stacked topological insulator built from bismuth-based graphene sheet analogues, *Nat. Mater.* **12**, 422 (2013).
- [7] P. Tang, B. Yan, W. Cao, S.-C. Wu, C. Felser, and W. Duan, Weak topological insulators induced by the inter-layer coupling: A first-principles study of stacked Bi_2Te_3 , *Phys. Rev. B* **89**, 041409(R) (2014).
- [8] G. Yang, J. Liu, L. Fu, W. Duan, and C. Liu, Weak topological insulators in PbTe/SnTe superlattices, *Phys. Rev. B* **89**, 085312 (2014).
- [9] C.-C. Liu, J.-J. Zhou, Y. Yao, and F. Zhang, Weak topological insulators and composite Weyl semimetals: $\beta\text{-Bi}_4\text{X}_4$ ($X = \text{Br}, \text{I}$), *Phys. Rev. Lett.* **116**, 066801 (2016).
- [10] Y. Zhang *et al.*, Electronic evidence of temperature-induced Lifshitz transition and topological nature in ZrTe_5 , *Nat. Commun.* **8**, 15512 (2017).
- [11] S. Liu *et al.*, Experimental observation of conductive edge states in weak topological insulator candidate HfTe_5 , *APL Mater.* **6**, 121111 (2018).
- [12] R. Noguchi *et al.*, A weak topological insulator state in quasi-one-dimensional bismuth iodide, *Nature (London)* **566**, 518 (2019).
- [13] J. Huang *et al.*, Room-temperature topological phase transition in quasi-one-dimensional material Bi_4I_4 , *Phys. Rev. X* **11**, 031042 (2021).

- [14] K. Lee *et al.*, Discovery of a weak topological insulating state and van Hove singularity in triclinic RhBi_2 , *Nat. Commun.* **12**, 1855 (2021).
- [15] Y. Ando, Topological insulator materials, *J. Phys. Soc. Jpn.* **82**, 102001 (2013).
- [16] J.-J. Zhou, W. Feng, C.-C. Liu, S. Guan, and Y. Yao, Large-gap quantum spin Hall insulator in single layer bismuth monobromide Bi_4Br_4 , *Nano Lett.* **14**, 4767 (2014).
- [17] J.-J. Zhou, W. Feng, G.-B. Liu, and Y. Yao, Topological edge states in single- and multi-layer Bi_4Br_4 , *New J. Phys.* **17**, 015004 (2015).
- [18] G. Autès *et al.*, A novel quasi-one-dimensional topological insulator in bismuth iodide $\beta\text{-Bi}_4\text{I}_4$, *Nat. Mater.* **15**, 154 (2016).
- [19] A. Pisoni, R. Gaal, A. Zeugner, V. Falkowski, A. Isaeva, H. Huppertz, G. Autes, O. V. Yazyev, and L. Forro, Pressure effect and superconductivity in $\beta\text{-Bi}_4\text{I}_4$ topological insulator, *Phys. Rev. B* **95**, 235149 (2017).
- [20] Y. Qi *et al.*, Pressure-induced superconductivity and topological quantum phase transitions in a quasi-one-dimensional topological insulator: Bi_4I_4 , *npj Quantum Mater.* **3**, 4 (2018).
- [21] X. Wang, J. Wu, J. Wang, T. Chen, H. Gao, P. Lu, Q. Chen, C. Ding, J. Wen, and J. Sun, Pressure-induced structural and electronic transitions in bismuth iodide, *Phys. Rev. B* **98**, 174112 (2018).
- [22] D.-Y. Chen *et al.*, Quantum transport properties in single crystals of $\alpha\text{-Bi}_4\text{I}_4$, *Phys. Rev. Mater.* **2**, 114408 (2018).
- [23] S. Deng, X. Song, X. Shao, Q. Li, Y. Xie, C. Chen, and Y. Ma, First-principles study of high-pressure phase stability and superconductivity of Bi_4I_4 , *Phys. Rev. B* **100**, 224108 (2019).
- [24] X. Li *et al.*, Pressure-induced phase transitions and superconductivity in a quasi-1-dimensional topological crystalline insulator $\alpha\text{-Bi}_4\text{Br}_4$, *Proc. Natl. Acad. Sci. U.S.A.* **116**, 17696 (2019).
- [25] C.-H. Hsu, X. Zhou, Q. Ma, N. Gedik, A. Bansil, V. M. Pereira, H. Lin, L. Fu, S.-Y. Xu, and T.-R. Chang, Purely rotational symmetry-protected topological crystalline insulator $\alpha\text{-Bi}_4\text{Br}_4$, *2D Mater.* **6**, 031004 (2019).
- [26] L. Qiao *et al.*, Ultralong single-crystal $\alpha\text{-Bi}_4\text{Br}_4$ nanobelts with a high current-carrying capacity by mechanical exfoliation, *J. Phys. Chem. C* **125**, 22312 (2021).
- [27] R. Noguchi *et al.*, Evidence for a higher-order topological insulator in a three-dimensional material built from van der Waals stacking of bismuth-halide chains, *Nat. Mater.* **20**, 473 (2021).
- [28] P. Wang, F. Tang, P. Wang, H. Zhu, C.-w. Cho, J. Wang, X. Du, Y. Shao, and L. Zhang, Quantum transport properties of $\beta\text{-Bi}_4\text{I}_4$ near and well beyond the extreme quantum limit, *Phys. Rev. B* **103**, 155201 (2021).
- [29] J. Zhuang, J. Li, Y. Liu, D. Mu, M. Yang, Y. Liu, W. Zhou, W. Hao, J. Zhong, and Y. Du, Epitaxial growth of quasi-one-dimensional bismuth-halide chains with atomically sharp topological non-trivial edge states, *ACS Nano* **15**, 14850 (2021).
- [30] X. Peng *et al.*, Observation of topological edge states on $\alpha\text{-Bi}_4\text{Br}_4$ nanowires grown on TiSe_2 substrates, *J. Phys. Chem. Lett.* **12**, 10465 (2021).
- [31] D.-Y. Chen, D. Ma, J. Duan, D. Chen, H. Liu, J. Han, and Y. Yao, Quantum transport evidence of boundary states and Lifshitz transition in Bi_4Br_4 , *Phys. Rev. B* **106**, 075206 (2022).
- [32] N. Shumiya *et al.*, Evidence of a room-temperature quantum spin Hall edge state in a higher-order topological insulator, *Nat. Mater.* **21**, 1111 (2022).
- [33] Y. Liu *et al.*, Gate-tunable transport in quasi-one-dimensional $\alpha\text{-Bi}_4\text{I}_4$ field effect transistors, *Nano Lett.* **22**, 1151 (2022).
- [34] M. Yang *et al.*, Large-gap quantum spin Hall state and temperature-induced Lifshitz transition in Bi_4Br_4 , *ACS Nano* **16**, 3036 (2022).
- [35] J. Zhong, M. Yang, F. Ye, C. Liu, J. Wang, J. Wang, W. Hao, J. Zhuang, and Y. Du, Facet-dependent electronic quantum diffusion in the high-order topological insulator Bi_4Br_4 , *Phys. Rev. Appl.* **17**, 064017 (2022).
- [36] X. Zhang *et al.*, Controllable epitaxy of quasi-one-dimensional topological insulator $\alpha\text{-Bi}_4\text{Br}_4$ for the application of saturable absorber, *Appl. Phys. Lett.* **120**, 093103 (2022).
- [37] E. V. Dikarev, B. A. Popovkin, and A. V. Shevelkov, New polymolecular bismuth monohalides. Synthesis and crystal structures of $\text{Bi}_4\text{Br}_x\text{I}_{4-x}$ ($x = 1, 2, \text{ or } 3$), *Russian chemical bulletin* **50**, 2304 (2001).
- [38] See Supplemental Material at <http://link.aps.org/supplemental/10.1103/PhysRevLett.133.086602>, which includes Refs. [39–55], for Topological material design concept; Crystal growth; Crystal structure analysis; ARPES setup; Sample preparation; Spin-resolved ARPES results; Band structure calculations; and Characterization of crystals used for potassium deposition experiments.
- [39] F. Tang, H. C. Po, A. Vishwanath, and X. Wan, Comprehensive search for topological materials using symmetry indicators, *Nature (London)* **566**, 486 (2019).
- [40] M. G. Vergniory, L. Elcoro, C. Felser, N. Regnault, B. A. Bernevig, and Z. Wang, A complete catalogue of high-quality topological materials, *Nature (London)* **566**, 480 (2019).
- [41] T. Zhang, Y. Jiang, Z. Song, H. Huang, Y. He, Z. Fang, H. Weng, and C. Fang, Catalogue of topological electronic materials, *Nature (London)* **566**, 475 (2019).
- [42] K. Yaji *et al.*, High-resolution three-dimensional spin- and angle-resolved photoelectron spectrometer using vacuum ultraviolet laser light, *Rev. Sci. Instrum.* **87**, 053111 (2016).
- [43] T. Shimojima, K. Okazaki, and S. Shin, Low-temperature and high-energy-resolution laser photoemission spectroscopy, *J. Phys. Soc. Jpn.* **84**, 072001 (2015).
- [44] P. Dudin, P. Lacovig, C. Fava, E. Nicolini, A. Bianco, G. Cautero, and A. Barinov, Angle-resolved photoemission spectroscopy and imaging with a submicrometre probe at the SPECTROMICROSCOPY-3.2L beamline of Elettra, *J. Synchrotron Radiat.* **17**, 445 (2010).
- [45] Y. Ishida and S. Shin, Functions to map photoelectron distributions in a variety of setups in angle-resolved photoemission spectroscopy, *Rev. Sci. Instrum.* **89**, 043903 (2018).
- [46] J. P. Perdew, K. Burke, and M. Ernzerhof, Generalized gradient approximation made simple, *Phys. Rev. Lett.* **77**, 3865 (1996).

- [47] G. Kresse and D. Joubert, From ultrasoft pseudopotentials to the projector augmented-wave method, *Phys. Rev. B* **59**, 1758 (1999).
- [48] G. Kresse and J. Hafner, *Ab initio* molecular dynamics for liquid metals, *Phys. Rev. B* **47**, 558 (1993).
- [49] G. Kresse and J. Hafner, *Ab initio* molecular-dynamics simulation of the liquid-metal–amorphous-semiconductor transition in germanium, *Phys. Rev. B* **49**, 14251 (1994).
- [50] G. Kresse and J. Furthmüller, Efficiency of *ab-initio* total energy calculations for metals and semiconductors using a plane-wave basis set, *Comput. Mater. Sci.* **6**, 15 (1996).
- [51] G. Kresse and J. Furthmüller, Efficient iterative schemes for *ab initio* total-energy calculations using a plane-wave basis set, *Phys. Rev. B* **54**, 11169 (1996).
- [52] N. Marzari and D. Vanderbilt, Maximally localized generalized Wannier functions for composite energy bands, *Phys. Rev. B* **56**, 12847 (1997).
- [53] I. Souza, N. Marzari, and D. Vanderbilt, Maximally localized Wannier functions for entangled energy bands, *Phys. Rev. B* **65**, 035109 (2001).
- [54] G. Pizzi *et al.*, Wannier90 as a community code: New features and applications, *J. Phys. Condens. Matter* **32**, 165902 (2020).
- [55] M. P. L. Sancho, J. M. L. Sancho, J. M. L. Sancho, and J. Rubio, Highly convergent schemes for the calculation of bulk and surface Green functions, *J. Phys. F* **15**, 851 (1985).
- [56] R. S. K. Mong, J. H. Bardarson, and J. E. Moore, Quantum transport and two-parameter scaling at the surface of a weak topological insulator, *Phys. Rev. Lett.* **108**, 076804 (2012).
- [57] Z. Ringel, Y. E. Kraus, and A. Stern, Strong side of weak topological insulators, *Phys. Rev. B* **86**, 045102 (2012).
- [58] L. Fu and C. L. Kane, Topology, delocalization via average symmetry and the symplectic Anderson transition, *Phys. Rev. Lett.* **109**, 246605 (2012).
- [59] Z.-H. Zhu *et al.*, Rashba spin-splitting control at the surface of the topological insulator Bi_2Se_3 , *Phys. Rev. Lett.* **107**, 186405 (2011).
- [60] P. D. C. King *et al.*, Large tunable Rashba spin splitting of a two-dimensional electron gas in Bi_2Se_3 , *Phys. Rev. Lett.* **107**, 096802 (2011).